On modeling the turbulent exchange in buoyancy-driven fronts

Gustavo M. Marques & Tamay M. Özgökmen

RSMAS, University of Miami

October 22, 2012

Outline

- OGCMs are the primary tools used for predicting ocean currents and the structure of the ocean's stratification;

Introduction

Importance of ocean general circulation models (OGCMs)

- OGCMs are the primary tools used for predicting ocean currents and the structure of the ocean's stratification;
- Significant development over the past two decades → facilitated by military's operational needs, industry (oil/gas) and basic research community;

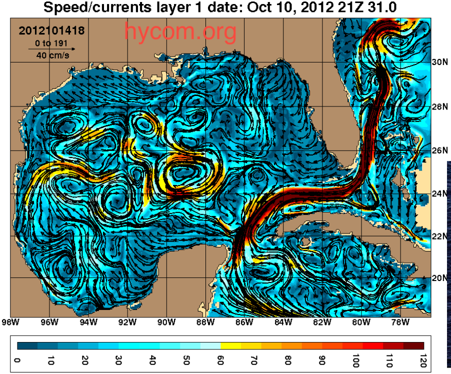

- Good representation of the observed energetics of mesoscale field using data-assimilation or high horizontal resolution $(1/25^o)$ (Thoppil et al., 2011 JGR) .

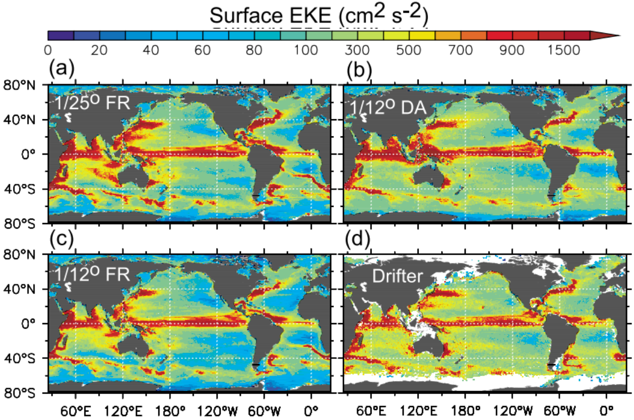

OGCMs may encounter significant obstacles due to primarily three reasons:

1. Data availability and technical challenges within the context of present assimilation methods;

OGCMs may encounter significant obstacles due to primarily three reasons:

1. Data availability and technical challenges within the context of present assimilation methods;
2. Accuracy of subgrid-scale (SGS) parameterizations when smaller features are not fully resolved;

OGCMs may encounter significant obstacles due to primarily three reasons:

1. Data availability and technical challenges within the context of present assimilation methods;
2. Accuracy of subgrid-scale (SGS) parameterizations when smaller features are not fully resolved;

OGCMs may encounter significant obstacles due to primarily three reasons:

1. Data availability and technical challenges within the context of present assimilation methods;
2. Accuracy of subgrid-scale (SGS) parameterizations when smaller features are not fully resolved;
3. Validity of primitive equations as $dx \rightarrow 0$, since hydrostatic approximation affects both dissipative and dispersive properties.

Objectives

Evaluate the mixing and stirring carried out by an OGCM (ROMS) under different modeling choices and similarly configured to a direct numerical simulation (DNS) or large eddy simulation (LES) model (**ground truth**).

Lock Exchange Problem for Stratified Mixing

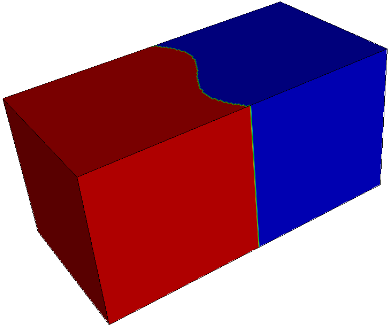

Upper Ocean Frontal Instability for Lateral Stirring

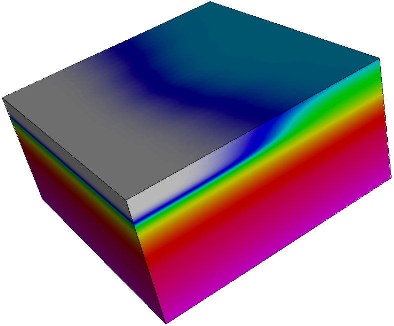

Non-dimensionalized Boussinesq equations:

$$
\begin{cases}
\dfrac{D\overline{\mathbf{u}}}{Dt} = \dfrac{1}{a\ Ro}\,\hat{\mathbf{z}} \times \overline{\mathbf{u}} - \nabla\overline{p} - Fr^{-2}\,\overline{\rho'}\,\hat{\mathbf{z}} + Re^{-1}\nabla^2\overline{\mathbf{u}} - \nabla\cdot\boldsymbol{\tau}\,, \\
\nabla\cdot\overline{\mathbf{u}} = 0\,, \\
\frac{D\overline{\rho'}}{Dt} = Pe^{-1}\nabla^2\overline{\rho'}\,, \\
\frac{D\overline{C}}{Dt} = Pe^{-1}\nabla^2\overline{C}\,,
\end{cases}
\tag{1}
$$

Non-dimensionalized Boussinesq equations:

$$\begin{cases} \frac{D\overline{\mathbf{u}}}{Dt} = \frac{1}{a\ Ro}\,\hat{\mathbf{z}} \times \overline{\mathbf{u}} - \nabla \overline{p} - Fr^{-2}\,\overline{\rho'}\,\hat{\mathbf{z}} + Re^{-1}\nabla^2\overline{\mathbf{u}} - \nabla \cdot \boldsymbol{\tau}\,, \\ \nabla \cdot \overline{\mathbf{u}} = 0\,, \\ \frac{D\overline{\rho'}}{Dt} = Pe^{-1}\nabla^2\overline{\rho'}\,, \\ \frac{D\overline{C}}{Dt} = Pe^{-1}\nabla^2\overline{C}\,, \end{cases} \tag{1}$$

$Re = U_0\,H_0/\nu$, $Ro = U_0/(f\,L)$, $a = L/H_0$,
$Fr = U_0/(N\,H_0)$, $Pe = RePr = U_0\,H_0/\kappa$ and $Pr = \nu/\kappa$.

Non-dimensionalized Boussinesq equations:

$$\begin{cases} \frac{D\overline{\mathbf{u}}}{Dt} = \frac{1}{a\ Ro}\,\hat{\mathbf{z}} \times \overline{\mathbf{u}} - \nabla\overline{p} - Fr^{-2}\,\overline{\rho'}\,\hat{\mathbf{z}} + Re^{-1}\nabla^2\overline{\mathbf{u}} - \nabla\cdot\boldsymbol{\tau}\,, \\ \nabla\cdot\overline{\mathbf{u}} = 0\,, \\ \frac{D\overline{\rho'}}{Dt} = Pe^{-1}\nabla^2\overline{\rho'}\,, \\ \frac{D\overline{C}}{Dt} = Pe^{-1}\nabla^2\overline{C}\,, \end{cases} \tag{1}$$

The subgrid scale tensor $\boldsymbol{\tau} = \overline{\mathbf{u}\mathbf{u}} - \bar{\mathbf{u}}\bar{\mathbf{u}}$ is computed using a **dynamic Smagorinsky model**, while no explicit subgrid models are used for the density perturbation and tracer concentration fields, relying instead on **de-aliasing** and **high-order filtering** operations.

Non-dimensionalized Boussinesq equations:

$$\begin{cases} \frac{D\overline{\mathbf{u}}}{Dt} = \frac{1}{a\ Ro}\,\hat{\mathbf{z}} \times \overline{\mathbf{u}} - \nabla\overline{p} - Fr^{-2}\,\overline{\rho'}\,\hat{\mathbf{z}} + Re^{-1}\nabla^2\overline{\mathbf{u}} - \nabla\cdot\boldsymbol{\tau}\,, \\ \nabla\cdot\overline{\mathbf{u}} = 0\,, \\ \frac{D\overline{\rho'}}{Dt} = Pe^{-1}\nabla^2\overline{\rho'}\,, \\ \frac{D\overline{C}}{Dt} = Pe^{-1}\nabla^2\overline{C}\,, \end{cases} \tag{1}$$

Further details can be found on Özgökmen et al., 2009a/b OM.

Primitive equations:

$$
\begin{cases}
\dfrac{\partial u}{\partial t} + \mathbf{u}\cdot\nabla u - fv = -\dfrac{1}{\rho_0}\dfrac{\partial \phi}{\partial x} + F_u + K_{MH}\nabla^2 u + \dfrac{\partial}{\partial z}(K_{MV}\dfrac{\partial u}{\partial z} + \nu\dfrac{\partial u}{\partial z}), \\
\frac{\partial v}{\partial t} + \mathbf{u}\cdot\nabla v + fu = -\frac{1}{\rho_0}\frac{\partial \phi}{\partial y} + F_v + K_{MH}\nabla^2 v + \frac{\partial}{\partial z}(K_{MV}\frac{\partial v}{\partial z} + \nu\frac{\partial v}{\partial z}), \\
\frac{\partial \phi}{\partial z} = -\frac{\rho' g}{\rho_0}, \\
\frac{\partial u}{\partial x} + \frac{\partial v}{\partial y} + \frac{\partial w}{\partial z} = 0, \\
\frac{\partial T}{\partial t} + \mathbf{u}\cdot\nabla T = F_T + K_{CH}\nabla^2 T + \frac{\partial}{\partial z}(K_{CV}\frac{\partial T}{\partial z} + \nu_\theta\frac{\partial T}{\partial z}), \\
\rho = \rho_0(1 - T_{coef} \times (T - T_0))
\end{cases}
\tag{2}
$$

Primitive equations:

$$
\begin{cases}
\frac{\partial u}{\partial t} + \mathbf{u}\cdot\nabla u - fv = -\frac{1}{\rho_0}\frac{\partial \phi}{\partial x} + F_u + K_{MH}\nabla^2 u + \frac{\partial}{\partial z}(K_{MV}\frac{\partial u}{\partial z} + \nu\frac{\partial u}{\partial z}), \\
\frac{\partial v}{\partial t} + \mathbf{u}\cdot\nabla v + fu = -\frac{1}{\rho_0}\frac{\partial \phi}{\partial y} + F_v + K_{MH}\nabla^2 v + \frac{\partial}{\partial z}(K_{MV}\frac{\partial v}{\partial z} + \nu\frac{\partial v}{\partial z}), \\
\frac{\partial \phi}{\partial z} = -\frac{\rho' g}{\rho_0}, \\
\frac{\partial u}{\partial x} + \frac{\partial v}{\partial y} + \frac{\partial w}{\partial z} = 0, \\
\frac{\partial T}{\partial t} + \mathbf{u}\cdot\nabla T = F_T + K_{CH}\nabla^2 T + \frac{\partial}{\partial z}(K_{CV}\frac{\partial T}{\partial z} + \nu_\theta\frac{\partial T}{\partial z}), \\
\rho = \rho_0(1 - T_{coef}\times(T - T_0))
\end{cases}
\tag{2}
$$

Horizontal momentum: third-order, upstream-biased advection scheme with velocity dependent hyper-viscosity (Shchepetkin and McWilliams, 1998 MWR).

Primitive equations:

$$\begin{cases} \frac{\partial u}{\partial t} + \mathbf{u} \cdot \nabla u - fv = -\frac{1}{\rho_0} \frac{\partial \phi}{\partial x} + F_u + K_{MH} \nabla^2 u + \frac{\partial}{\partial z} (K_{MV} \frac{\partial u}{\partial z} + \nu \frac{\partial u}{\partial z}), \\ \frac{\partial v}{\partial t} + \mathbf{u} \cdot \nabla v + fu = -\frac{1}{\rho_0} \frac{\partial \phi}{\partial y} + F_v + K_{MH} \nabla^2 v + \frac{\partial}{\partial z} (K_{MV} \frac{\partial v}{\partial z} + \nu \frac{\partial v}{\partial z}), \\ \frac{\partial \phi}{\partial z} = -\frac{\rho' g}{\rho_0}, \\ \frac{\partial u}{\partial x} + \frac{\partial v}{\partial y} + \frac{\partial w}{\partial z} = 0, \\ \frac{\partial T}{\partial t} + \mathbf{u} \cdot \nabla T = F_T + K_{CH} \nabla^2 T + \frac{\partial}{\partial z} (K_{CV} \frac{\partial T}{\partial z} + \nu_\theta \frac{\partial T}{\partial z}), \\ \rho = \rho_0 (1 - T_{coef} \times (T - T_0)) \end{cases} \tag{2}$$

Vertical momentum: fourth-order centered differences scheme.

Primitive equations:

$$
\begin{cases}
\frac{\partial u}{\partial t} + \mathbf{u} \cdot \nabla u - fv = -\frac{1}{\rho_0}\frac{\partial \phi}{\partial x} + F_u + K_{MH}\nabla^2 u + \frac{\partial}{\partial z}(K_{MV}\frac{\partial u}{\partial z} + \nu\frac{\partial u}{\partial z}), \\
\frac{\partial v}{\partial t} + \mathbf{u} \cdot \nabla v + fu = -\frac{1}{\rho_0}\frac{\partial \phi}{\partial y} + F_v + K_{MH}\nabla^2 v + \frac{\partial}{\partial z}(K_{MV}\frac{\partial v}{\partial z} + \nu\frac{\partial v}{\partial z}), \\
\frac{\partial \phi}{\partial z} = -\frac{\rho' g}{\rho_0}, \\
\frac{\partial u}{\partial x} + \frac{\partial v}{\partial y} + \frac{\partial w}{\partial z} = 0, \\
\frac{\partial T}{\partial t} + \mathbf{u} \cdot \nabla T = F_T + K_{CH}\nabla^2 T + \frac{\partial}{\partial z}(K_{CV}\frac{\partial T}{\partial z} + \nu_\theta\frac{\partial T}{\partial z}), \\
\rho = \rho_0(1 - T_{coef} \times (T - T_0))
\end{cases}
\tag{2}
$$

Tracers: advected using a recursive Multidimensional Positive Definite Advection Transport Algorithm (MPDATA) scheme.

Primitive equations:

$$\begin{cases} \dfrac{\partial u}{\partial t} + \mathbf{u}\cdot\nabla u - fv = -\dfrac{1}{\rho_0}\dfrac{\partial \phi}{\partial x} + F_u + K_{MH}\nabla^2 u + \dfrac{\partial}{\partial z}(K_{MV}\dfrac{\partial u}{\partial z} + \nu\dfrac{\partial u}{\partial z}), \\ \frac{\partial v}{\partial t} + \mathbf{u}\cdot\nabla v + fu = -\frac{1}{\rho_0}\frac{\partial \phi}{\partial y} + F_v + K_{MH}\nabla^2 v + \frac{\partial}{\partial z}(K_{MV}\frac{\partial v}{\partial z} + \nu\frac{\partial v}{\partial z}), \\ \frac{\partial \phi}{\partial z} = -\frac{\rho' g}{\rho_0}, \\ \frac{\partial u}{\partial x} + \frac{\partial v}{\partial y} + \frac{\partial w}{\partial z} = 0, \\ \frac{\partial T}{\partial t} + \mathbf{u}\cdot\nabla T = F_T + K_{CH}\nabla^2 T + \frac{\partial}{\partial z}(K_{CV}\frac{\partial T}{\partial z} + \nu_\theta\frac{\partial T}{\partial z}), \\ \rho = \rho_0(1 - T_{coef} \times (T - T_0)) \end{cases} \tag{2}$$

Horizontal mixing of momentum and tracers are computed using a **Laplacian** formulation.

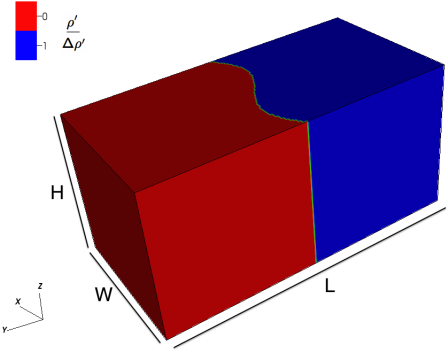

Nek5000, **DNS** (Özgökmen et al., 2009 OM)

- $a = L/H_0 = 2$ and $W/H_0 = 1$;
- $Fr = \frac{0.5\sqrt{g\Delta\rho' H/\rho_0}}{\sqrt{g\Delta\rho' 0.5H/\rho_0}} = 2^{-1/2}$;
- $Ro = 0$, $Pr = 7$;
- $Re = 10^3$ and 10^4.

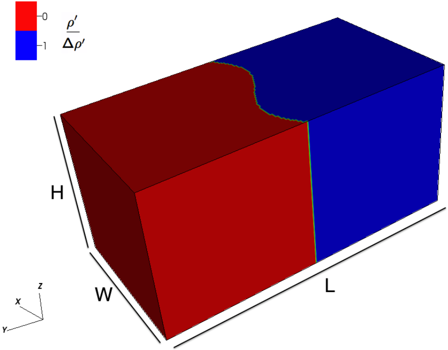

ROMS

- $L = 200$ m and $W = H_0 = 100$ m $\rightarrow$ a $= L/H_0 = 2$;
- $Fr = 2^{-1/2}$, $Ro = 0$;
- $Pr_H = 7$, $Re_H = 10^3$ and 10^4;
- Re_V and Pr_V $\rightarrow$ closure.

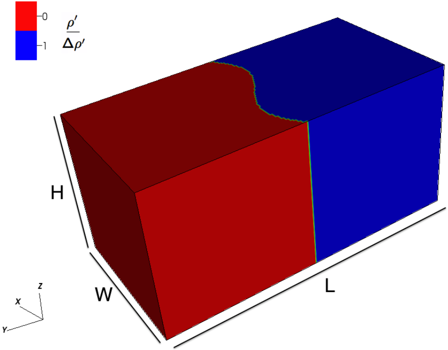

DNS/ROMS

Boundary Conditions:

- EW $\rightarrow$ periodic;
- NS $\rightarrow$ no-flow and free-slip;
- No bottom friction.

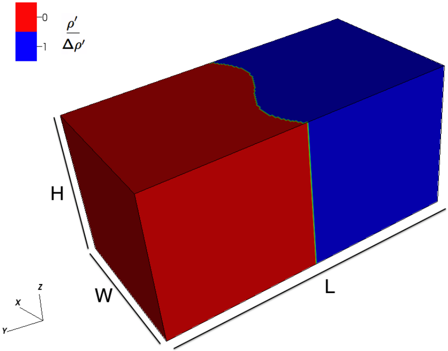

DNS/ROMS

Boundary Conditions:

- EW $\rightarrow$ periodic;
- NS $\rightarrow$ no-flow and free-slip;
- No bottom friction.

Initial Conditions:

- $\mathbf{u} = 0$;

$$\frac{\rho'(x,y,z,0)}{\Delta\rho'} = \begin{cases} 1 & \text{for } 0 \geq x < (L/2+\eta), \\ 0 & \text{for } (L/2+\eta) \geq x \leq L. \end{cases}$$

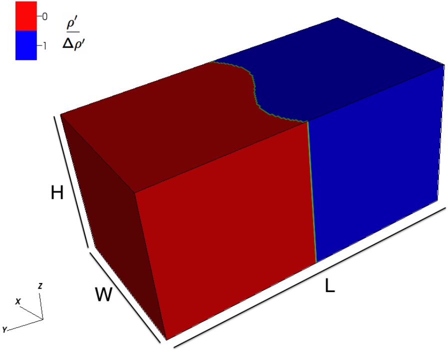

DNS/ROMS

Time scale for the system:

- $T_p = L/(0.5\sqrt{g\Delta\rho' H/\rho_0})$.

Total integration period:

- $t^* = 4 \times T/T_p \sim 60$.

	Exp.	Re_H	Turbulence closure
10 m	le-res10A	10^3	k-ε/CA
	le-res10B	10^3	KPP
5 m	le-res5A	10^3	k-ε/CA
	le-res5B	10^3	KPP
2.5 m	le-res2.5A	10^3	k-ε/CA
	le-res2.5B	10^3	KPP
	le-res2.5E*	10^3	k-ε/CA
1.25 m	le-res1.25A	10^3	k-ε/CA
	le-res1.25B	10^3	KPP
	le-res1.25C	10^4	k-ε/CA
	le-res1.25D	10^4	KPP
	le-res1.25F	10^3	none
	le-res1.25G	10^4	none
	le-res1.25H	10^3	none

1. grid resolution;

U3H
C4V

Exp.	Re_H	Turbulence closure
le-res10A	10^3	k-ε/CA
le-res10B	10^3	KPP
le-res5A	10^3	k-ε/CA
le-res5B	10^3	KPP
le-res2.5A	10^3	k-ε/CA
le-res2.5B	10^3	KPP
le-res2.5E*	10^3	k-ε/CA
le-res1.25A	10^3	k-ε/CA
le-res1.25B	10^3	KPP
le-res1.25C	10^4	k-ε/CA
le-res1.25D	10^4	KPP
le-res1.25F	10^3	none
le-res1.25G	10^4	none
le-res1.25H	10^3	none

1. grid resolution;
2. tracer advection scheme;

Exp.	Re_H	Turbulence closure
le-res10A	10^3	k-ε/CA
le-res10B	10^3	KPP
le-res5A	10^3	k-ε/CA
le-res5B	10^3	KPP
le-res2.5A	10^3	k-ε/CA
le-res2.5B	10^3	KPP
le-res2.5E*	10^3	k-ε/CA
le-res1.25A	10^3	k-ε/CA
le-res1.25B	10^3	KPP
le-res1.25C	10^4	k-ε/CA
le-res1.25D	10^4	KPP
le-res1.25F	10^3	none
le-res1.25G	10^4	none
le-res1.25H	10^3	none

1. grid resolution;
2. tracer advection scheme;
3. explicit Re_H;

Exp.	Re_H	Turbulence closure
le-res10A	10^3	k-ε/CA
le-res10B	10^3	KPP
le-res5A	10^3	k-ε/CA
le-res5B	10^3	KPP
le-res2.5A	10^3	k-ε/CA
le-res2.5B	10^3	KPP
le-res2.5E*	10^3	k-ε/CA
le-res1.25A	10^3	k-ε/CA
le-res1.25B	10^3	KPP
le-res1.25C	10^4	k-ε/CA
le-res1.25D	10^4	KPP
le-res1.25F	10^3	none
le-res1.25G	10^4	none
le-res1.25H	10^3	none

1. grid resolution;
2. tracer advection scheme;
3. explicit Re_H;
4. choice of turbulence closures;

Lock Exchange Problem for Stratified Mixing

List of experiments and quantification of mixing

Exp.	Re_H	Turbulence closure
le-res10A	10^3	k-ε/CA
le-res10B	10^3	KPP
le-res5A	10^3	k-ε/CA
le-res5B	10^3	KPP
le-res2.5A	10^3	k-ε/CA
le-res2.5B	10^3	KPP
le-res2.5E*	10^3	k-ε/CA
le-res1.25A	10^3	k-ε/CA
le-res1.25B	10^3	KPP
le-res1.25C	10^4	k-ε/CA
le-res1.25D	10^4	KPP
le-res1.25F	10^3	none
le-res1.25G	10^4	none
le-res1.25H	10^3	none

Vertical visc/diff=0

1. grid resolution;
2. tracer advection scheme;
3. explicit Re_H;
4. choice of turbulence closures;
5. control experiments.

Contours of normalized density perturbation $\rho'/\Delta\rho'$

ROMS

res=1.25 m, Re_H=10^4 and $k-\epsilon$/CA

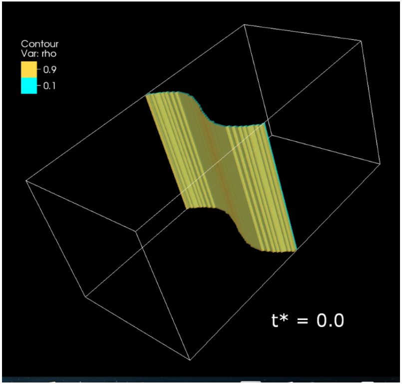

DNS

Re=10^4

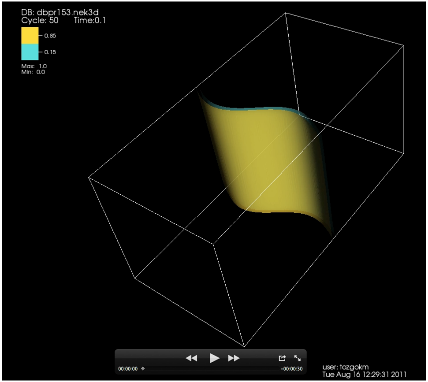

Contours of normalized density perturbation $\rho'/\Delta\rho'$

ROMS

res=1.25 m, Re_H=10^4 and $k-\epsilon$/CA

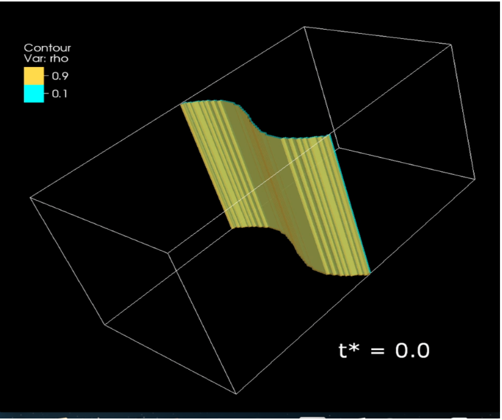

DNS

Re=10^4

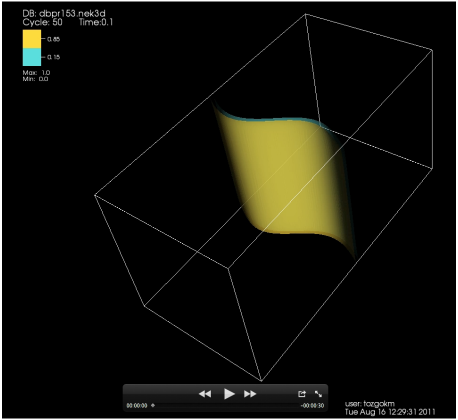

Compute **background** (or reference) **potential energy** (**BPE**), which **quantifies mixing** in a enclosed system (Winters et al., 1995 JFM) following Tseng and Ferziger, (2001, PF) by using **probability density function**:

$$BPE = gLW \int_0^H \rho'(z_r) z_r dz_r, \quad (3)$$

where $z_r(\rho')$ is the **height** of fluid of density ρ' in the **minimum potential energy state**.

Non-dimensional background potential energy:

$$BPE^*(t^*) = \frac{BPE(t^*) - BPE(0)}{BPE(0)} \quad (4)$$

10 m res., different turbulence closures and $Re_H = \mathbf{10^3}$

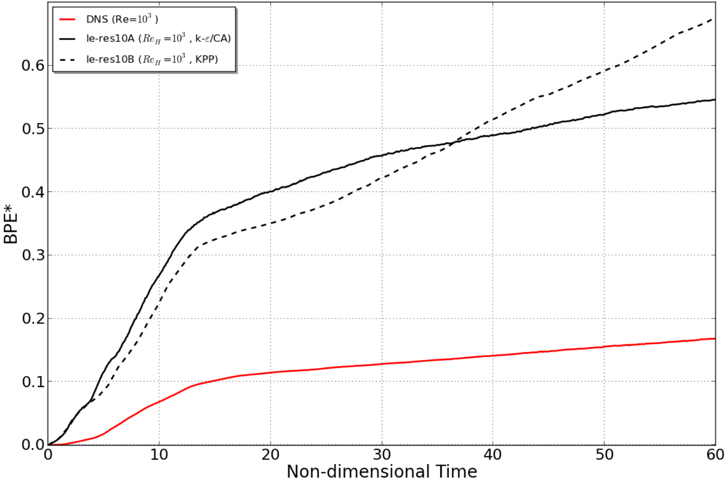

5, **2.5** and **1.25** m res., different turbulence closures and $Re_H = \mathbf{10^3}$

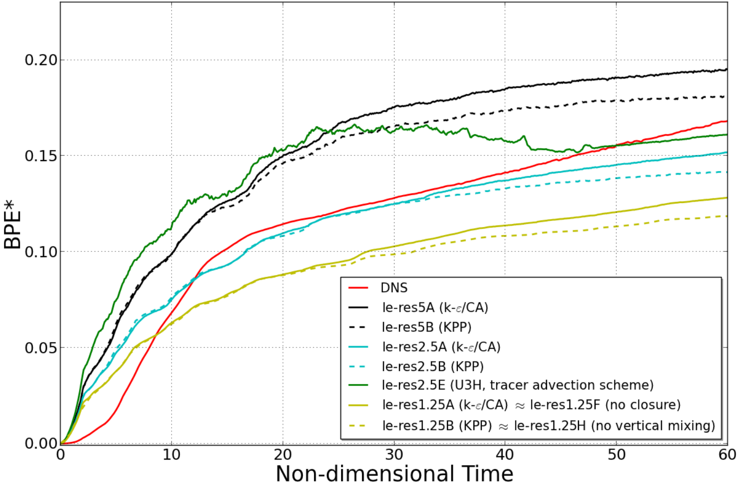

1.25 m res., different turbulence closures and $Re_H = \mathbf{10^4}$

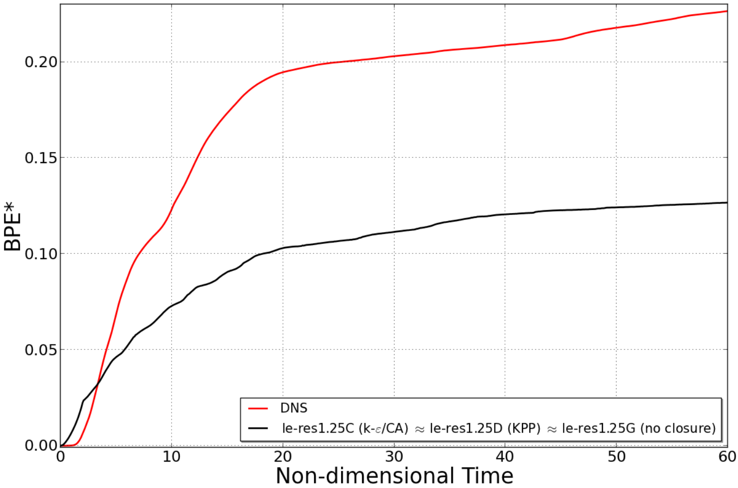

Normalized root-mean-square error: $\epsilon = \frac{\sqrt{\frac{1}{n}\sum_{i=0}^{n}(BPE_{DNS} - BPE_{ROMS})^2}}{max(BPE_{DNS})}$

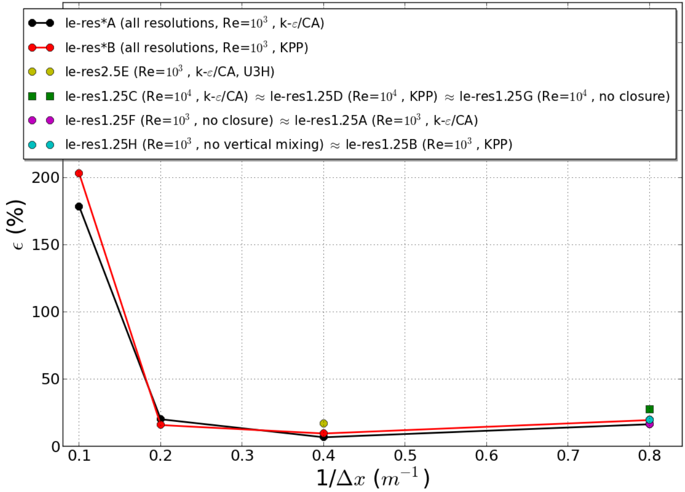

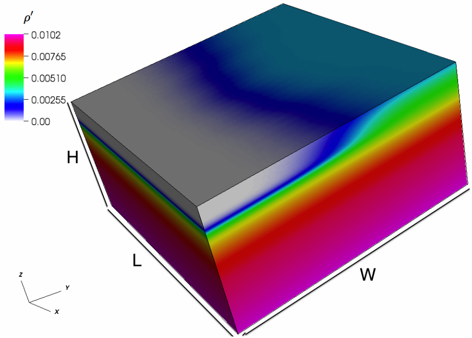

Nek5000, **LES** (Özgökmen et al., 2011 OM)

- a $= L/H_0 = W/H_0 = 20$;
- Fr $= 0.1$;
- Pr $= 7$;
- Re $= 10^5$;
- Ro=0.02.

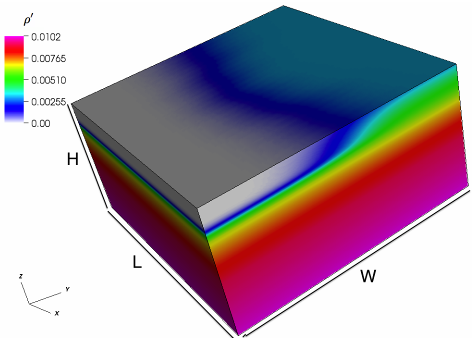

ROMS

- $L = W = 10$ km and $H_0 = 500$ m $\rightarrow$ a $= 20$;
- $N \approx 4.42 \times 10^{-4} s^{-1}$;
- $U_0 \approx 0.02$ m/s;
- $Fr = U_0/(NH_0) \approx 0.1$;
- $f = 1.21 \times 10^{-4}\ s^{-1}$;
- $Ro = U_0/(fL) \approx 0.02$

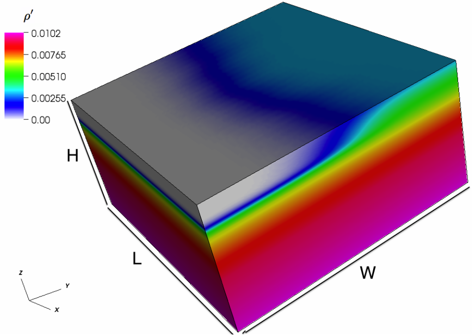

LES/ROMS

- Fastest growing modes R;
- ML radius of deformation $R_d = \sqrt{\frac{g}{\rho_0}\Delta\rho'_m h_o}/f$;
- Assume $R/R_d \approx 5$ (Eldevik and Dysthe, 2002 JPO);
- $R_d \approx 400$ m and $R \approx 2$ km.

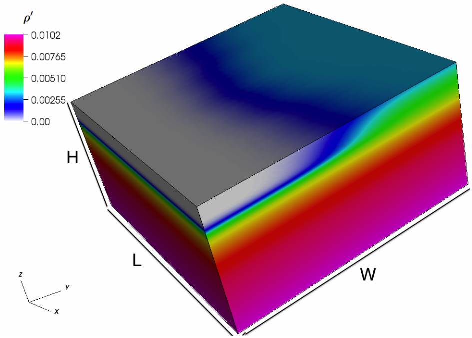

LES/ROMS

Boundary Conditions:

- EW → periodic;
- NS → no-flow and free-slip;
- No bottom friction.

Exp.	N_σ	Δx=$\Delta y(m)$	min/max Δz (m)	Turb. closure
mli-01	32	100	3.1/160.6	k-ε/CA
mli-02	32	200	3.1/160.6	k-ε/CA
mli-03	32	50	3.1/160.6	k-ε/CA
mli-04	16	100	6.3/259.1	k-ε/CA
mli-05	64	100	1.6/90.1	k-ε/CA
mli-06	32	100	3.1/160.6	KPP
mli-c1	32	100	3.1/160.6	none

1. horizontal resolution;

Exp.	N_σ	Δx=$\Delta y(m)$	min/max Δz (m)	Turb. closure
mli-01	32	100	3.1/160.6	k-ε/CA
mli-02	32	200	3.1/160.6	k-ε/CA
mli-03	32	50	3.1/160.6	k-ε/CA
mli-04	16	100	6.3/259.1	k-ε/CA
mli-05	64	100	1.6/90.1	k-ε/CA
mli-06	32	100	3.1/160.6	KPP
mli-c1	32	100	3.1/160.6	none

1. horizontal resolution;
2. choice of turbulence closure;

Exp.	N_σ	Δx=$\Delta y(m)$	min/max Δz (m)	Turb. closure
mli-01	32	100	3.1/160.6	k-ε/CA
mli-02	32	200	3.1/160.6	k-ε/CA
mli-03	32	50	3.1/160.6	k-ε/CA
mli-04	16	100	6.3/259.1	k-ε/CA
mli-05	64	100	1.6/90.1	k-ε/CA
mli-06	32	100	3.1/160.6	KPP
mli-c1	32	100	3.1/160.6	none

1. horizontal resolution;
2. choice of turbulence closure;
3. control exp.;

Exp.	N_σ	Δx=$\Delta y(m)$	min/max Δz (m)	Turb. closure
mli-01	32	100	3.1/160.6	k-ε/CA
mli-02	32	200	3.1/160.6	k-ε/CA
mli-03	32	50	3.1/160.6	k-ε/CA
mli-04	16	100	6.3/259.1	k-ε/CA
mli-05	64	100	1.6/90.1	k-ε/CA
mli-06	32	100	3.1/160.6	KPP
mli-c1	32	100	3.1/160.6	none

1. horizontal resolution;
2. choice of turbulence closure;
3. control exp.;
4. vertical resolution.

Vtrans=1, **Vstretch**=1, $\theta_\mathbf{s}$=16, $\theta_\mathbf{b}$=0 and **TCLINE** = 100 m.

ρ' (kg/m^3) for experiment mli-01 (dx=100 m, kϵ/CA, N$_\sigma$=32)

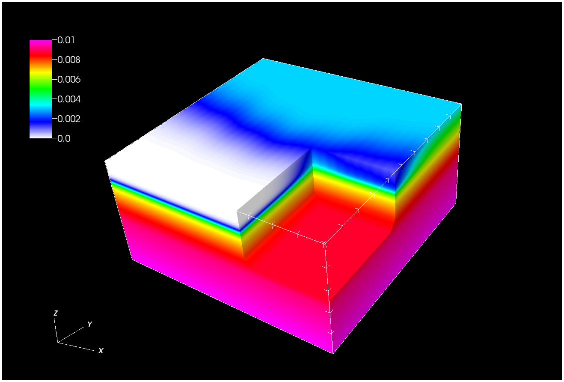

- Oscillations around the geostrophically adjusted state (Tandon and Garrett, 1994 JPO);
- No significant changes in stratification during this period (Boccaletti et al., 2007 JPO);
- MLIs are visible and restratification begins after a few days;
- Coherent vortices with $R \approx 2$ km.

ρ' (kg/m^3) for experiment mli-01 (dx=100 m, kϵ/CA, N$_\sigma$=32)

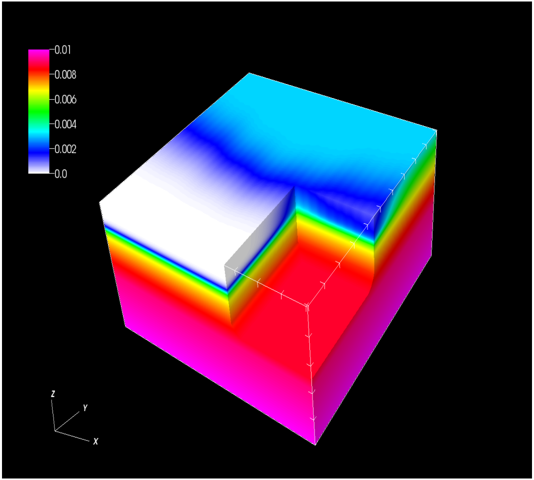

- Oscillations around the geostrophically adjusted state (Tandon and Garrett, 1994 JPO);
- No significant changes in stratification during this period (Boccaletti et al., 2007 JPO);
- MLIs are visible and restratification begins after a few days;
- Coherent vortices with $R \approx 2$ km.

ρ' (kg/m^3) at time $=$ 15 days

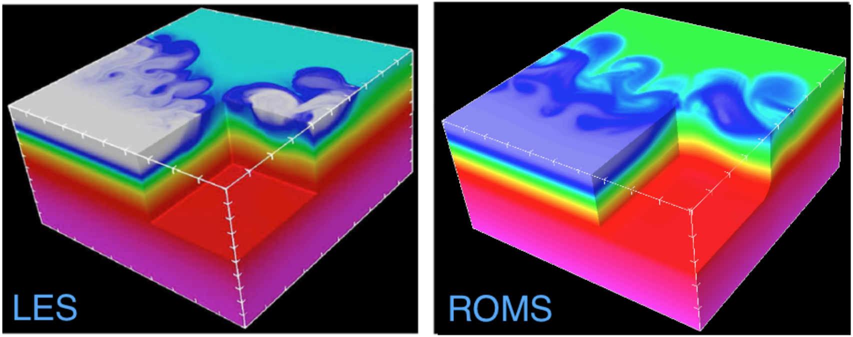

LES 3D ρ' field is visually very similar to the ROMS simulations.

Passive tracer (kg/m^3) field for exp. mli-01 (dx=100 m, $k\epsilon$/CA, N_σ=32)

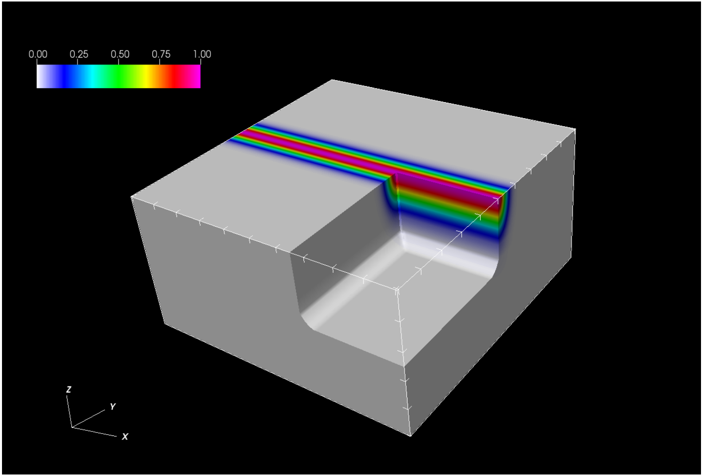

Passive tracer (kg/m^3) field for exp. mli-01 (dx=100 m, kϵ/CA, N_σ=32)

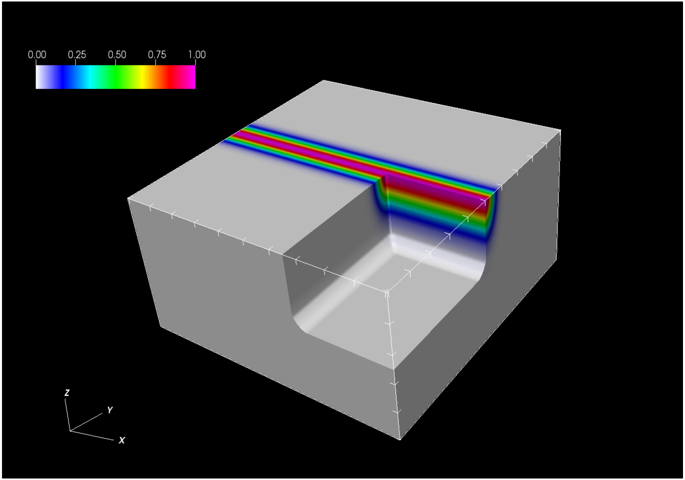

Second moment (or tracer variance) of the tracer field (C) across the front and at a fixed level of $z_0 = 5$ m:

$$\sigma_y^2(t, z_0) = \frac{M_{02}(t, z_0) - M_{01}^2(t, z_0)}{M_{00}(t, z_0)} \quad (3)$$

where

$$M_{mp}(t, z_0) = \frac{1}{A} \int \int x^m y^p C(x, y, z_0, t) dxdy. \quad (4)$$

This is frequently employed in the analysis of observational data (Sundermeyer and Ledwell, 2001 JPO).

Upper Ocean Frontal Instability for Lateral Stirring

Results: comparison between LES and ROMS

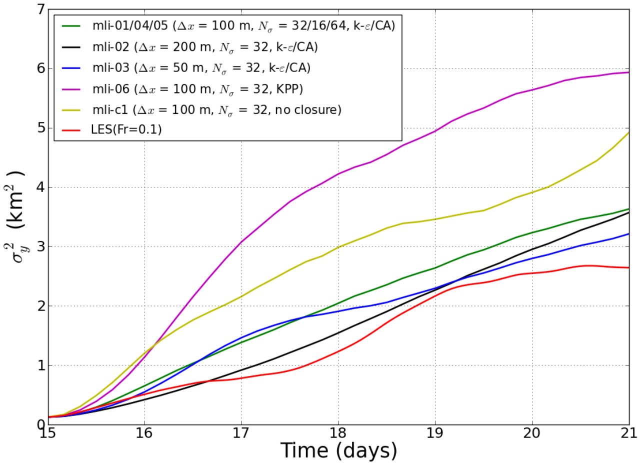

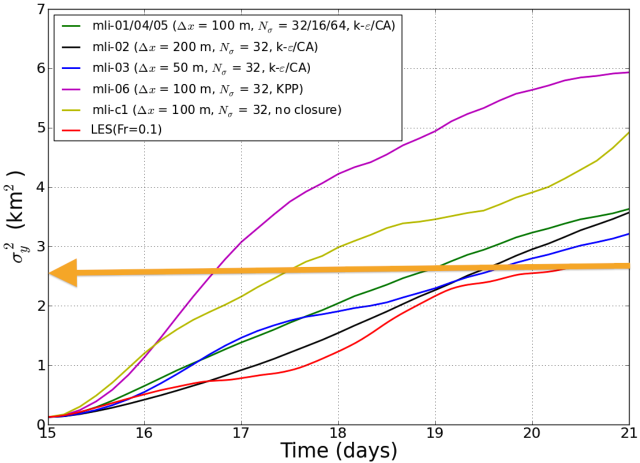
mli-01/04/05 (Δx = 100 m, N_σ = 32/16/64, k-ε/CA)
mli-02 (Δx = 200 m, N_σ = 32, k-ε/CA)
mli-03 (Δx = 50 m, N_σ = 32, k-ε/CA)
mli-06 (Δx = 100 m, N_σ = 32, KPP)
mli-c1 (Δx = 100 m, N_σ = 32, no closure)
LES(Fr=0.1)
σ_y^2 (km^2)
Time (days)
0
1
2
3
4
5
6
7
15
16
17
18
19
20
21

Tracer variance starting at time = 0 days

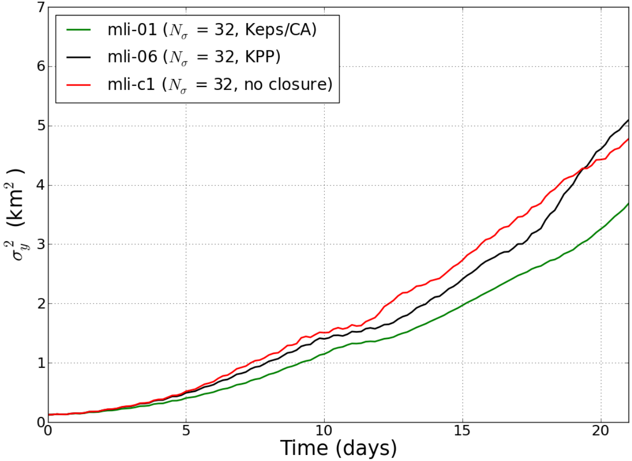

Eddy stream function ψ_e (Mahadevan et al, 2010 JGR)

$$\psi_e = \epsilon \left(\frac{\epsilon \ \overline{v'b'} \ \overline{b_z} - \epsilon^{-1} \ \overline{w'b'} \ \overline{b_y}}{\overline{b_y}^2 + \epsilon^2 \overline{b_z}^2} \right) \quad (3)$$

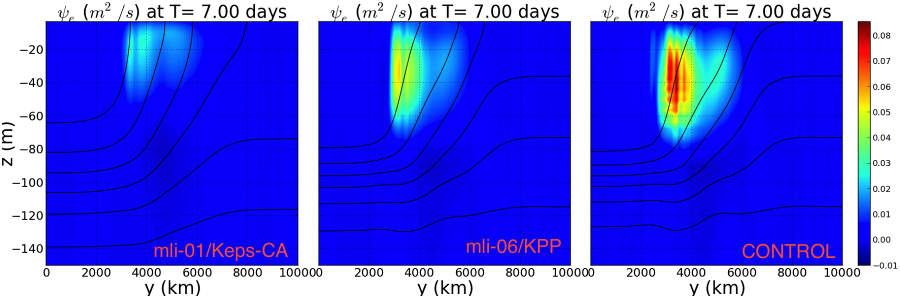

Maximum ψ_e (m^2/s) in the mixed layer versus time (days)

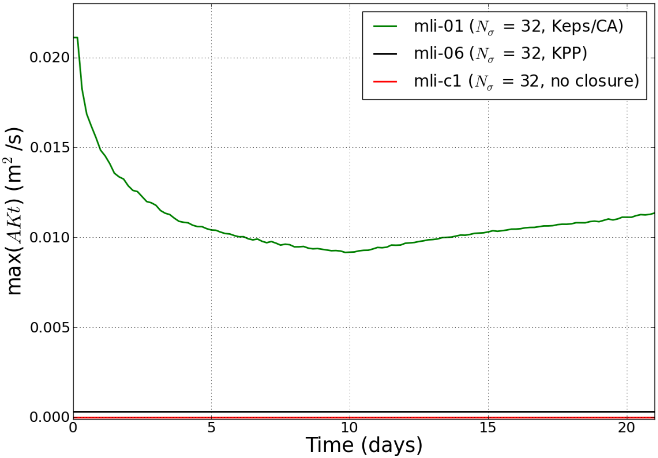

Max. vertical diffusivity AKt (m^2/s) in the mixed layer versus time (days)

Going back to σ_y^2 computations from tracer release at day 15.

The y-component of (effective) diffusivity can be obtained following:

$$K_y = \frac{1}{2}\frac{\partial \sigma_y^2}{\partial t}. \tag{3}$$

Use 6 hrs interval and then compute normalized root-mean-square error:

$$\epsilon = \frac{\sqrt{\frac{1}{n}\sum_{i=0}^{n}(K_{y-LES} - K_{y-ROMS})^2}}{max(K_{y-LES}) - min(K_{y-LES})} \tag{4}$$

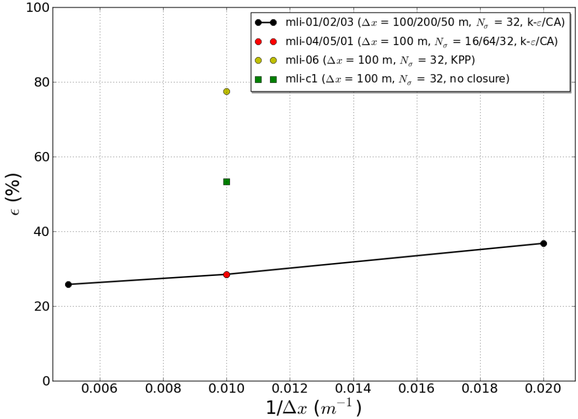

Exp.	$< K_y > \ (m^2/s)$
LES	2.0
mli-01	3.4
mli-02	3.3
mli-03	3.0
mli-04	3.3
mli-05	3.5
mli-06	5.8
mli-c1	4.5

Values are within the limits observed over the c. shelf on spatial scales of 1-10 km and timescales of less then 5 days (Sundermeyer and Ledwell, 2001 JPO).

- No convergence is attained towards the DNS as $\Delta x \to 0$ and the best results are achieved with an intermediate resolution of 2.5 m;

- No convergence is attained towards the DNS as $\Delta x \to 0$ and the best results are achieved with an intermediate resolution of 2.5 m;
- U3H/C4V tracer scheme overestimates mixing (and gives a non-monotonic behavior). The results are improved by ∼10 % when using MPDATA.

- $k - \epsilon / CA$ gives good agreement with LES; poor performance of KPP due to extremely low vertical viscosity/diffusivity $\rightarrow$ faster restratification;

- $k - \epsilon/CA$ gives good agreement with LES; poor performance of KPP due to extremely low vertical viscosity/diffusivity $\rightarrow$ faster restratification;
- To our knowledge, the importance of the turbulence closure on mixed layer restratification has been identified for the first time.

Acknowledgements

Thank you!

Questions?